2025 23rd European Control Conference (ECC)
June 24-27, 2025. Thessaloniki, Greece

Optimal Power Smoothing of Airborne Wind Energy Systems via Pseudo-Spectral Methods and Multi-objective Analysis

Mattia Alborghetti, Filippo Trevisi, Roberto Boffadossi, Lorenzo Fagiano

***Abstract*— The problem of optimizing the power output of a class of Airborne Wind Energy Systems (AWES), named fly-gen, is considered. Fly-gen AWES, called windplanes in this paper, harvest wind power by means of an autonomous tethered aircraft that carries out periodic trajectories roughly perpendicular to the wind flow (crosswind conditions), using onboard turbines and converters and an electric tether to transfer power to the ground. The amount of generated power and its variability strongly depend on the flown trajectory, whose optimization is a highly nonlinear and non-convex problem. Differently from most of the existing literature on the topic, this problem is here addressed from a multi-objective perspective, where both the average power and its variability are considered. Through a recently-proposed pseudo-spectral decomposition of the states and inputs, a rather small-scale nonlinear program is derived to obtain a periodic orbit that maximizes the average power under a constraint on its variability. Then, a series of such programs is formulated and solved to approximate the Pareto front of the problem. Finally, the latter is exploited to analyze the possible trade-offs. The main finding of this work is that, contrary to what postulated so far in the scientific community, it is possible to operate the windplane with minimal power fluctuations (10% of the average) with a very small reduction of mean power, of the order of 5% with respect to the maximum achievable. Additional considerations regarding the sensitivity of the optimal trajectories to various factors are presented, too. These results pave the way for a completely novel way of optimizing and controlling windplanes.**

I. Introduction

Airborne Wind Energy Systems (AWES) employ tethered, fully autonomous airborne devices to generate electricity. The most promising concepts fly the airborne units crosswind [1] and can be classified into ground-gen and fly-gen systems [2], [3]. This paper focuses on fly-gen systems, called windplanes in this paper, which generate power with relatively small onboard turbines and send it to the ground station via the tether (Fig. 1). A typical flight path for these systems is shaped like a loop [4], even though figure-eight patterns have been proposed as well [5].

The most notable prototypes of fly-gen systems were developed by Makani Power, which stopped operations in 2020 [4]. Their prototypes experienced large power fluctuations over the crosswind loop, often using the turbines as propellers in the ascending part of the loop [4]. A control scheme, including a temperature controller and the possibility to overload the powertrain temporarily, is proposed over the entire wind speed range [5]. Recently, a new design methodology for windplanes has been proposed [6], resulting in a low aspect ratio wing and conventional, efficient airfoils. However, also in [6] the resulting flight path presents a rather large power variability. In this work, an optimal control approach and a multi-objective analysis are proposed to search for the Pareto front of flown trajectories with various trade-offs in terms of average power and variability. This task is particularly challenging due to the system nonlinearities and non-convexity of the resulting optimization problems. To alleviate these problems, a pseudo-spectral decomposition of the states' and inputs' trajectories is employed and an harmonic balance approach is adopted [7]. This kind of approach has been successfully applied in related research fields, such as wave energy converters (WECs), where it has

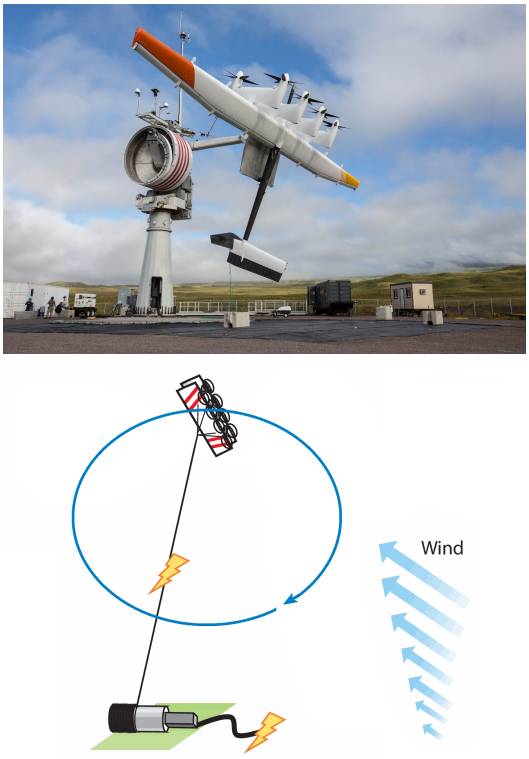

Fig. 1: Top: Makani Power prototype [4]. Bottom: fly-gen or onboard-generation Airborne Wind Energy concept.

M. Alborghetti, F. Trevisi, R.Boffadossi and L. Fagiano are with the Department of Electronics, Information and Bioengineering, Politecnico di Milano, Piazza Leonardo da Vinci 32, 20133 Milano, Italy. Email: {name.surname}@polimi.it; R.Boffadossi is also with the Institute of Intelligent Industrial Technologies and Systems for Advanced Manufacturing (STIIMA), National Research Council, Via Alfonso Corti, 12, 20133 Milano, Italy. Email: {name.surname}@stiima.cnr.it

This research has been supported by Fondazione Cariplo under grant n. 2022-2005, project "NextWind - Advanced control solutions for large scale Airborne Wind Energy Systems", by the Italian Ministry of University and Research under grants "DeepAirborne - Advanced Modeling, Control and Design Optimization Methods for Deep Offshore Airborne Wind Energy" (NextGenerationEU fund, project P2022927H7), the Extended Partnership "NEST - Network 4 Energy Sustainable Transition" and by the MERIDIONAL project, which receives funding from the European Union's Horizon Europe Programme under the grant agreement No. 101084216.

proven advantageous in terms of computational efficiency and ease of implementation [8]. Notably, it enables the computation of optimal periodic trajectories, even under strong nonlinearities and complex constraints. Alternatively, [9] proposes a time-domain optimal control solution for AWE systems, employing various homotopy strategies to construct effective initial guesses.

For the sake of completeness, note that also for ground-gen systems, a control to smooth the power fluctuation has been studied [10]. However, ground-gen systems cannot avoid large power fluctuations due to the so-called pumping cycle, where the tether is periodically reeled out under large forces and the reeled in by actually spending energy. Fly-gen systems do not have this inconvenience.

The main application-oriented contribution of this work is to show, for the first time in the literature, that optimal trajectories with extremely limited power fluctuations at a negligible cost in terms of average produced power do exist. Ensuring a smoothed power output is crucial to meet grid connection requirements. Moreover, it prevents the need for oversizing electrical generators, intermediate energy storage devices, and power conversion systems, thereby reducing costs and improving the overall system efficiency [11].

Only circular-based trajectories are here analyzed, but the same methodology can be applied to eight-path shapes.

II. System Description and Modeling

A Fly-gen Airborne Wind Energy System (AWES), called windplane in this paper, is an aircraft-like device that generates wind power by flying in fast crosswind motion. Equipped with onboard generators and tethered to a ground station, it converts wind energy into electricity, transmitting it to the ground through a conductive tether. The main elements are

- **The ground station:** This includes foundational mechanical structures, a winch for tether management, and energy conversion systems connected to the grid or storage. Additionally, it contains sensors, communication systems, and control interfaces.
- **The tether:** A multi-layered, durable cable, containing conductive materials for electrical power transmission.
- **The aircraft:** A rigid-wing structure equipped with onboard generators, actuators, control surfaces, sensors, and a communication system.

The system operates through different phases that ultimately lead to the power generation stage. These include take-off, landing, and the transitions between these and the generation phase. This work focuses specifically on the power production phase, during which the windplane flies in cyclic circular or figure-eight trajectories, and the onboard turbines convert wind energy into electrical power.

In this paper, the windplane is modeled as a point mass in space. Since the tether is treated as a rigid link, the motion is constrained in a sphere of radius equal to the tether length. Therefore, the system can be modeled with two degrees of freedom, as in [7]. The states are then the angular positions $z(t) = \left[\beta(t),\ \phi(t)\right]^T$ in the spherical coordinate system (Fig. 2). The model in [7] is here upgraded with modified control inputs and an improved aerodynamic model. The control inputs are

$$u(t) = \left[\psi(t),\ a_t(t),\ C_L(t)\right]^T. \tag{1}$$

The roll angle ψ, as defined in [7], approximates the roll angle of the aircraft and can be controlled with the ailerons. The onboard wind turbines induction a_t determines the turbines thrust and power and can be controlled by modifying the angular velocity of the rotors. Finally, C_L is the wing lift coefficient and can be controlled by actuating the elevator (or the entire horizontal stabilizer).

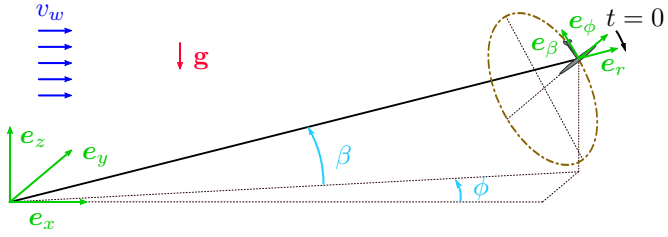

Fig. 2: Sketch of the geometry. Inertial coordinate system $(\mathbf{e}_x, \mathbf{e}_y, \mathbf{e}_z)$ and spherical coordinate system $(\mathbf{e}_r, \mathbf{e}_\phi, \mathbf{e}_\beta)$.

Denoting three-dimensional-component space vectors with bold symbols, the model dynamics read

$$\boldsymbol{f} = \boldsymbol{L} + \boldsymbol{D} + \boldsymbol{T}_t + \boldsymbol{F}_g + \boldsymbol{T} - m\boldsymbol{a} = \boldsymbol{0}. \tag{2}$$

$\boldsymbol{L}$ is the aerodynamic lift. $\boldsymbol{D}$ is the aerodynamic drag, inclusive of the equivalent tether drag and of the airfoils polars [6]. $\boldsymbol{T}_t$ is the turbines' thrust, defined as

$$\boldsymbol{T}_t = \frac{1}{2}\rho A_t C_{T,t} \left|\boldsymbol{v}_a\right| \boldsymbol{v}_a, \tag{3}$$

with $C_{T,t} = 4a_t(1 - a_t)$ and the apparent velocity $\boldsymbol{v}_a$ is composed by the free stream velocity $\boldsymbol{v}_w$, the induced velocity from the far wake $\boldsymbol{v}_{i,f}$ and the plane velocity $\boldsymbol{v}$: $\boldsymbol{v}_a = \boldsymbol{v}_w + \boldsymbol{v}_{i,f} - \boldsymbol{v}$. The induced velocities due to the far wake $\boldsymbol{v}_{i,f} = -a_f v_w \cos\hat{\beta}\mathbf{e}_{\hat{\beta}}$ are estimated with a vortex model [12] and implemented with the formulation in [6]. The induction due to the far wake a_f is then

$$a_f = \frac{\kappa_0^{\pi/2}}{4\pi} \frac{\hat{C}_T \hat{\lambda}^2}{\left(\hat{\lambda} - \hat{C}_T\right)^{3/2}}, \tag{4}$$

where $\kappa_0 = (b/2)/\hat{R}$, with b being the wingspan and $\hat{R}$ the average turning radius, $\hat{\lambda} = \hat{v}/(v_w \cos\hat{\beta})$ is the mean wing speed ratio and the thrust coefficient $\hat{C}_T$

$$\hat{C}_T = \frac{\widehat{\boldsymbol{L} \cdot \boldsymbol{v}_w}}{P_{\text{ref}}} \tag{5}$$

where P_{ref} is

$$P_{\text{ref}} = \frac{1}{2}\rho\pi b^2 v_w^3. \tag{6}$$

The remaining external forces in Eq. 2 are the gravitational force $\boldsymbol{F}_g$ and the tether force $\boldsymbol{T}$, acting radially. Finally, m is the windplane mass and $\boldsymbol{a}$ its acceleration.

The windplane shaft power is

$$P(t) = \frac{1}{2}\rho A_t C_{P,t}(t) |\boldsymbol{v}_a|^3(t), \tag{7}$$

where $A_t = N_t \pi R_t^2$ is the onboard wind turbine total area, $C_{P,t} = 4a_t(1-a_t)^2$ is the onboard turbine power coefficient, defined using momentum theory, and v_a is the apparent wind velocity seen by the onboard turbines. Finally, the shaft mechanical power can be converted into electrical power by reducing it by the electrical efficiency $P_e = \eta P$.

III. Multi-objective pseudo-spectral optimal control problem formulation

The model dynamics described in Section II can be written as a set of second-order nonlinear differential equations in the form

$$\boldsymbol{f}(z(t), \dot{z}(t), \ddot{z}(t), u(t)) = \mathbf{0}, \tag{8}$$

where $z(t)$ is the state vector and $u(t)$ is the control vector. By assuming that Eq. (8) accepts periodic solutions, every state variable is expanded as a Fourier series of order N_z and of fundamental frequency $\omega = 2\pi/\tau$, with τ being the trajectory period

$$\begin{aligned} z(t) &\approx \hat{Z} + \sum_{k=1}^{N_z} Z_{k,s} \sin(k\omega t) + Z_{k,c} \cos(k\omega t), \\ Z &= \left[\hat{Z},\ Z_{1,s},\ Z_{2,s},\ \dots, Z_{1,c},\ Z_{2,c},\ \dots\right]^T. \end{aligned} \tag{9}$$

Similarly, each control input is expanded as a Fourier series of order N_u as

$$\begin{aligned} u(t) &\approx \hat{U} + \sum_{k=1}^{N_u} U_{k,s} \sin(k\omega t) + U_{k,c} \cos(k\omega t), \\ U &= \left[\hat{U},\ U_{1,s},\ U_{2,s},\ \dots, U_{1,c},\ U_{2,c},\ \dots\right]^T. \end{aligned} \tag{10}$$

The equations of motion (Eq. 8) can also be expanded as Fourier series of order N_z as

$$\begin{aligned} \boldsymbol{f} &\approx \hat{F} + \sum_{k=1}^{N_z} F_{k,s} \sin(k\omega t) + F_{k,c} \cos(k\omega t), \\ F &= \left[\hat{F},\ F_{1,s},\ F_{2,s},\ \dots, F_{1,c},\ F_{2,c},\ \dots\right]^T. \end{aligned} \tag{11}$$

According to the harmonic balance method, the model dynamics in Eq. (8) are respected if all its Fourier coefficients F, which are function of the Fourier coefficients of the states Z and of the control inputs U and of the fundamental frequency ω, are null

$$F(Z, U, \omega) = 0. \tag{12}$$

A multi-objective trajectory optimization framework, which employs the pseudo-spectral formulation just introduced, is developed to identify the optimal control inputs to maximize the mean power production while minimizing harmonic oscillations. The optimization variables are the Fourier coefficients of the states and the inputs, along with the fundamental angular frequency

$$x = \left[Z_\beta,\ Z_\phi,\ U_\psi,\ U_{at},\ U_{CL},\ \omega\right]. \tag{13}$$

Multi-objective Optimization Problems (MOPs) aim to optimize all elements in a vector of conflicting scalar objective functions, resulting in a set of Pareto-optimal solutions, also known as non-dominated solutions [13]. For each of these solutions, no other feasible alternative can improve the performance of one objective without degrading another, according to the Pareto dominance relationship [14]. The corresponding points in the criterion space constitute the *Pareto front*, which illustrates the trade-off curve, i.e. the different alternatives in optimizing the considered objectives. The MOP employed for trajectory optimization is defined as follows

$$\begin{aligned} \min_{x \in \mathcal{X}} \quad & \left[-\hat{P}(x), \Delta P(x)\right] \\ \text{s.t.} \quad & F(x) = 0. \end{aligned} \tag{14}$$

where the objectives are the average power produced over a period $\hat{P}(x)$ and the harmonic power content $\Delta P(x)$. The equality constraints are the Fourier coefficient of the model dynamics F (Eq. 12). The harmonic power content $\Delta P(x)$ is efficiently defined in the frequency domain as

$$\begin{aligned} \Delta P(x) &= \|P_{\text{harm}}\|_2, \\ P_{\text{harm}} &= \left[P_{1,s},\ P_{2,s},\ \dots, P_{1,c},\ P_{2,c},\ \dots\right]^T, \end{aligned} \tag{15}$$

with P_{harm} being the vector containing the Fourier coefficients of the power, excluding the mean value.

This study performs a comprehensive trade-off analysis, rather than computing a single solution that achieves a desired balance between the two objectives. Thus, a sufficiently representative solution set for the entire *Pareto optimal set* and the corresponding Pareto front in the criterion space (i.e. a posterior articulation of preferences [14]) is here provided. To enhance convergence and achieve a uniform distribution of solutions, deterministic classical methods are chosen over evolutionary algorithms [15] and, more generally, over metaheuristics [16]. Specifically, the ε-constraint scalarization approach [17] is used, enabling the separation of the scalar objectives of the considered bi-criteria problem, unlike other widely used scalarization methods such as the weighted sum [18], normal constraint [19], Normal-Boundary Intersection [20], Pascoletti-Serafini [21].

The optimization problem formulation in Eq. (14) is then reformulated as

$$\begin{aligned} \min_{x \in \mathcal{X}} \quad & -\hat{P}(x) \\ \text{s.t.} \quad & \Delta P(x) \leq \varepsilon \\ & F(x) = 0. \end{aligned} \tag{16}$$

The maximization of power production is chosen as the primary goal and the minimization of harmonic oscillation is converted into an additional constraint. Furthermore, the ε parameter is varied uniformly within the range defined by the two anchor points, obtaining a well-distributed point-cloud approximation of the Pareto front.

The resulting single-objective instances of the ε-constraint problem formulation, defined in Eq. (16), are constrained, single-objective, non-linear and non-convex optimization problems with $N_{z,tot} + N_{u,tot} + 1$ optimization variables and $N_{z,tot}$ number of equality constraints. With

$$\begin{aligned} N_{z,tot} &= 2(N_\beta + N_\phi) + 2 \\ N_{u,tot} &= 2(N_\psi + N_{at} + N_{CL}) + 3. \end{aligned} \tag{17}$$

In order to solve them the standard interior-point gradient-based solver provided in the *fmincon* MATLAB function is used. The initial guesses are taken to be circular trajectories found with analytical approximations. The derivatives of

the flight dynamic model with respect to the optimization variables are taken analytically and provided to the solver, allowing for a deep and fast convergence of the solution. The problem instances are solved using an AMD Ryzen 9 (3.79 GHz) 12-core processor with 32 GB of RAM. Each solution takes approximately 10 seconds of computational time.

Remark 1: The frequency domain formulation of the control problem offers several advantages over its time-domain approach for this system. It inherently captures periodic behavior without requiring additional constraint, as would be needed in the time domain. Moreover, time domain parametrization can quickly escalate the number of optimization variables as the period τ grows, while in the frequency domain, the number of variables remains fixed, influenced solely by the number of harmonics. This could be sufficiently low for effective engineering control of such systems.

IV. Main Analyses and Findings

To carry out all the analyses of this paper, a system of 100 kW rated power and 10 m wingspan has been designed by improving the design proposed in [6]. Its characteristics are shown in Table I. Moreover, the order of the number of optimization variables is determined to be as in Table II.

Parameter	Value
P_r (rated power)	100 kW
b (wingspan)	10 m
AR (aspect ratio)	6.4
airfoil	FFA-W3 211
m (mass)	245 kg
L_{te} (tether length)	150 m
D_{te} (tether diameter)	10 mm
$C_{d,te}$ (tether drag coefficient)	1
N_t (number of turbines)	2
R_t (turbine radius)	1.25 m

TABLE I: System parameters.

N_z		N_u	
N_β	10	N_ψ	2
N_ϕ	10	N_{at}	2
		N_{CL}	1

TABLE II: Number of harmonics for states and controls used throughout the paper simulations.

A. Multi-objective problem in idealized condition

This subsection presents the trade-off analyses for an idealized condition with constant wind speed of $v_w = 7$ m/s. The windplane can fly at negative elevation angles, which would be unfeasible in a real application because of the presence of the ground. This idealization allows to understand key physical phenomena also present in more realistic cases, analyzed later.

The Pareto front under these idealized conditions is depicted in Figure 3, highlighting key Pareto-optimal solutions to be compared. For clarity, the criterion space was filtered to exclude negligible solutions—either dominated or non-dominated points that deviate from the typical shape of the estimated front. Due to this operation, the presented solutions are not classified as globally Pareto optimal. Moreover, the assessment of their global Pareto optimality exceeds the scope of this analysis.

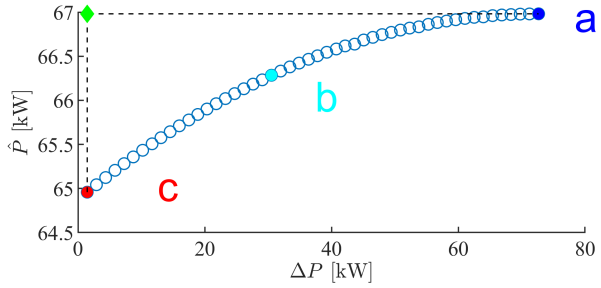

Fig. 3: Pareto front approximation in nominal case ($v_w = 7$ m/s).

The utopia point in Figure 3 is represented as a green diamond, while the light blue point *b* denotes the compromise solution computed after normalizing the objectives relative to the corresponding worst-performing Pareto-optimal solution (i.e. point *b* represents the solution having the smallest Euclidean distance from the utopia point in the normalized criterion space). The anchor point *a* corresponds to the optimal solution obtained by maximizing the mean power without constraints on the power fluctuation; in this condition, the corresponding mean power $\hat{P}^a$ is the maximum achievable. The anchor point *c* corresponds to the optimal solution obtained by constraining the power fluctuation to be $\Delta P \leq 0.02\ \hat{P}^a$. To evaluate the performance of various Pareto-optimal solutions, Figure 4 illustrates simulation trends for cases *a*, *b*, and *c* over one cycle period τ.

The results indicate that power fluctuation can be minimized at a slight cost in average power (at most 2 kW), while keeping comparable control effort. The lift coefficient C_L influences the average power through its mean value, while its fluctuation is approximately set to be opposite with respect to the plane velocity [6] for aerodynamic reasons. The roll angle ψ is set to redirect lift upward and compensate gravity [7]. The turbine induction a_t plays a crucial role in reducing ΔP. Looking at the anchor point *a*, the turbine induction a_t is set to convert part of the gravitational power to electrical power. Indeed, at $t = 0$ the windplane points downward, thus the effect of gravitational force is reduced by the increased turbines' thrust force. This is found to be optimal for the mean power [7], [6]. Looking at the anchor point *c*, the turbine induction a_t is instead set to keep the power $P(t)$ (Eq. 7) constant. In order to achieve a constant power, the product between the onboard wind turbine power coefficient $C_{P,t} = 4a_t(1-a_t)^2$ shall be at the maximum value when the windplane velocity v, and thus the apparent velocity cubed v_a^3, is at the minimum value. To minimize power fluctuation, the phase of a_t is then adjusted to be anti-phased with the windplane speed v. The windplane trajectories remain closely similar (Figure 5). Note that, without an elevation constraint, the optimal trajectory has $\hat{\beta} < 0$ because in this case the wing is almost purely crosswind [7]. Thus, for all these reasons, the decision-maker may prefer solution

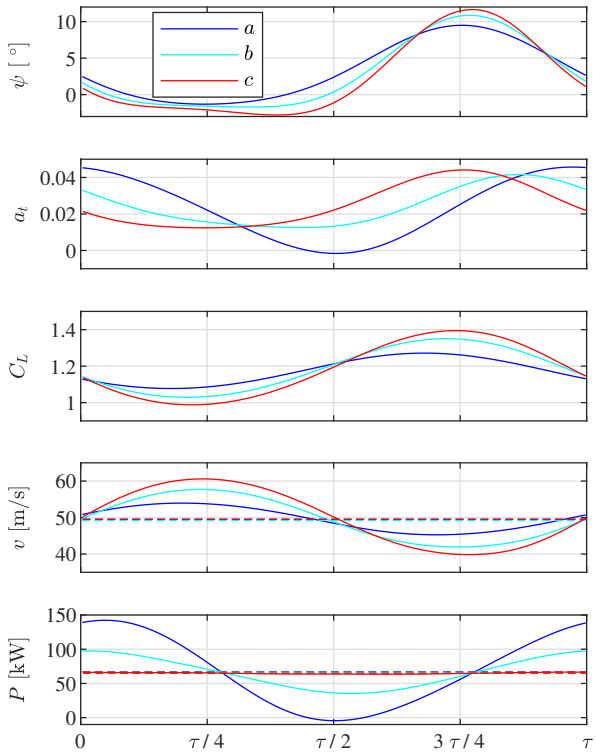

Fig. 4: Comparison of Pareto-optimal solutions in nominal case ($v_w = 7$ m/s). ψ, a_t, C_L are the control inputs. v is the windplane speed and P the shaft power. Average values are in dashed lines. The periods are τ_a = 7.4 s, τ_b = 7.3 s, τ_c = 7.2 s.

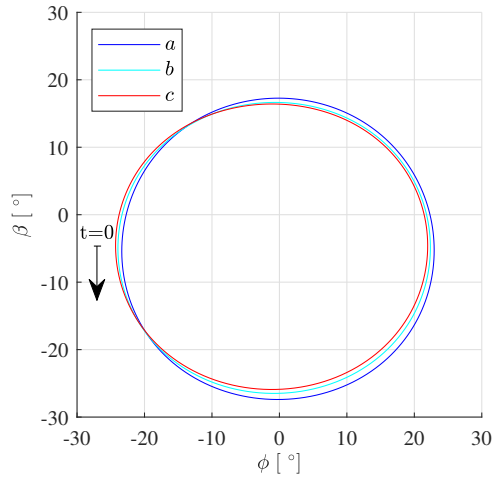

Fig. 5: Windplane space trajectories comparison of key Pareto-optimal solutions in nominal case ($v_w = 7$ m/s).

c, which emphasizes reducing power oscillation ΔP with a small mean power penalty.

B. Sensitivity analyses for different wind speeds and mean elevation angles

In this subsection, the sensitivity of the Pareto curve under varying wind speeds (assumed constant with altitude) and different elevation angles is studied. The optimal control problem (14) is then enlarged with an equality constraint on the mean elevation angle $\hat{\beta}$. This ensures that the windplane flies safely above ground and can also be used for power-curtailment grid strategy. Using the frequency-domain parametrization, the mean elevation can be enforced simply by fixing the first Fourier coefficient of the elevation angle.

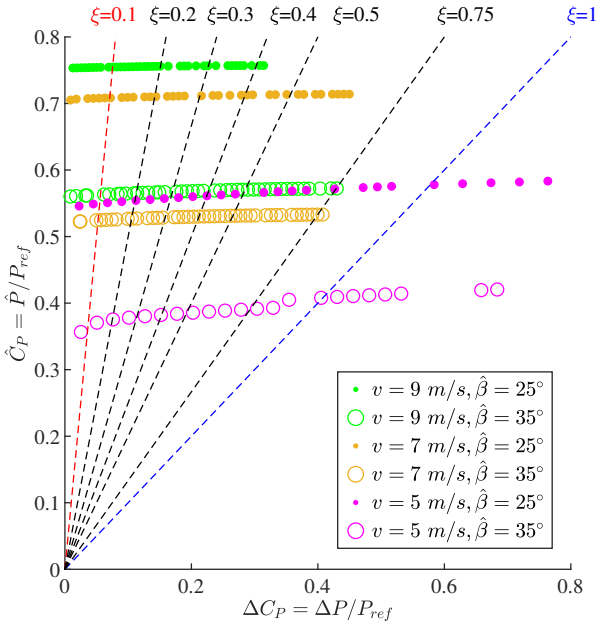

Fig. 6: Normalized Pareto fronts approximation at different wind conditions and mean elevation angles. Dashed lines represent the equation $\hat{C}_P = \xi \Delta C_P$

The windplane under consideration starts to produce energy at the cut-in wind speed of approximately $v_w \approx 5$ m/s and reaches rated power at approximately $v_w \approx 9$ m/s, with a mean elevation angle $\hat{\beta} \approx 30°$. For this reason, the system is studied at $v_w = 5$ m/s, at $v_w = 7$ m/s and at $v_w = 9$ m/s. Two reasonable use-case mean elevation angles are considered $\hat{\beta} = 25°$ and $\hat{\beta} = 35°$. In order to clearly show the Pareto fronts, the mean power $\hat{P}$ and its fluctuation ΔP are normalized with a reference power P_{ref} corresponding to the wind power passing through a disk with radius equal to the wingspan b (Eq. 6) [6]. The conclusions obtained in Section IV-A are broadly generalizable as shown in Figure 6. Indeed, the resulting curves obtained from the computed Pareto optimal solutions are relatively flat, indicating that the power oscillations can be minimized without a substantial decrease in average power for the investigated v_w and $\hat{\beta}$. This normalized power $\hat{P}/P_{\text{ref}}$, referred as the power coefficient $\hat{C}_P$ in [6], is representative of the efficiency of the power conversion from wind power to electrical power. This power coefficient reaches higher values for higher wind speeds because the power losses due to the exchange of gravitational

potential energy decrease [6]. Moreover, higher power can be harvested at lower elevation angles, as can be noted by comparing the solutions at the same incoming wind speed. Figure 6 shows also a few dashed lines starting from the origin. The solutions on the left of these lines are characterized by a power fluctuation lower than the indicated value ξ times the mean power. As an example, a solution lying on the left to the line closest to the y-axis ($\xi = 0.1$) has a power fluctuation lower than 10 % of the mean power $\Delta P < 0.1\ \hat{P}$. Note that operating the system to be on the right of $\xi = 1$ presents two main drawbacks: (1) using the onboard turbines as propellers, when $P(t) < 0$. This dual-use scenario is generally suboptimal because consuming power leads to a double-count of the electrical efficiency and thus a large reduction of the mean generated power [7]; (2) high power excursions necessitate an oversized electric generator, increasing costs and onboard mass, negatively affect overall windplane performance. The sensitivity analysis carried out in this section shows that the power fluctuations can be reduced without large mean power reduction at all relevant below-rated wind speeds. In particular, it is possible to reduce the harmonic power content to 10 % of the mean power by reducing the power production up to 5% with respect to the maximum achievable for all the analyzed cases.

V. Conclusions and Outlook

This paper provides an in-depth analysis on the power production of Airborne Wind Energy Systems (AWES), introducing an enhanced system model and a novel multi-objective optimal control problem to the literature. A frequency-domain parametrization, utilizing the harmonic balance method, is applied to significantly reduce optimization variables compared to time-domain methods. Through a comprehensive trade-off analysis, a power smoothing policy is demonstrated and quantified, significantly reducing power fluctuations—by at least 10% of the average— while maintaining a comparable control effort and only slightly reducing the mean power (up to 5% compared to the maximum achievable). This holds across wind speeds between the cut-in and rated wind speeds, with elevation angles that ensure safety from ground and power curtailment strategies. A key insight reveals that power smoothing is driven by the harmonic control of onboard turbine induction, which needs to be in anti-phase with respect to the windplane velocity. Future research will extend the analysis to eight-path-shapes AWES trajectory and global Pareto fronts through global optimization techniques. Other multi-objective formulations will also be considered, such as minimizing tether force oscillations, which affect structural loads and durability. Importantly, the optimal trajectories from the power smoothing policy will serve as a foundation for the derivation of feedback control strategies and multi-objective predictive control studies. An extension to a six-degree-of-freedom model is currently under investigation to evaluate closed-loop performance under actuator dynamics.

References

[1] M. Loyd, "Crossswind kite power," *Journal of Energy*, vol. 4, no. 3, pp. 106–111, 1980.

[2] C. Vermillion, M. Cobb, L. Fagiano, R. Leuthold, M. Diehl, R. S. Smith, T. A. Wood, S. Rapp, R. Schmehl, D. Olinger, and M. Demetriou, "Electricity in the air: Insights from two decades of advanced control research and experimental flight testing of airborne wind energy systems," *Annual Reviews in Control*, vol. 52, pp. 330–357, 2021.

[3] L. Fagiano, M. Quack, F. Bauer, L. Carnel, and E. Oland, "Autonomous airborne wind energy systems: Accomplishments and challenges," *Annual Review of Control, Robotics, and Autonomous Systems*, vol. 5, no. Volume 5, 2022, pp. 603–631, 2022.

[4] P. Echeverri, T. Fricke, G. Homsy, and N. Tucker, "The energy kite. selected results from the design, development and testing of makani's airborne wind turbines. part i." Makani Technologies LLC, Tech. Rep., 2020, available at https://x.company/projects/makani/.

[5] F. Bauer, D. Petzold, R. M. Kennel, F. Campagnolo, and R. Schmehl, "Control of a drag power kite over the entire wind speed range," *Journal of Guidance, Control, and Dynamics*, vol. 42, no. 10, pp. 2167–2182, 2019.

[6] F. Trevisi, "Conceptual design of windplanes," PhD thesis, Politecnico di Milano, 2024, available at https://hdl.handle.net/10589/216694.

[7] F. Trevisi, I. Castro-Fernández, G. Pasquinelli, C. E. D. Riboldi, and A. Croce, "Flight trajectory optimization of fly-gen airborne wind energy systems through a harmonic balance method," *Wind Energy Science*, vol. 7, no. 5, pp. 2039–2058, 2022.

[8] A. Mérigaud, "A harmonic balance framework for the numerical simulation of non-linear wave energy converter models in random seas," Ph.D. dissertation, 2018. [Online]. Available: https://mural.maynoothuniversity.ie/id/eprint/10861/

[9] J. De Schutter, R. Leuthold, T. Bronnenmeyer, E. Malz, S. Gros, and M. Diehl, "Awebox: An optimal control framework for single- and multi-aircraft airborne wind energy systems," *Energies*, vol. 16, no. 4, 2023. [Online]. Available: https://www.mdpi.com/1996-1073/16/4/1900

[10] J. Hummel, T. Pollack, D. Eijkelhof, E. V. Kampen, and R. Schmehl, "Power smoothing by kite tether force control for megawatt-scale airborne wind energy systems," *Journal of Physics: Conference Series*, vol. 2767, no. 7, p. 072019, jun 2024.

[11] R. Joshi, D. von Terzi, M. Kruijff, and R. Schmehl, "Techno-economic analysis of power smoothing solutions for pumping airborne wind energy systems," *Journal of Physics: Conference Series*, vol. 2265, no. 4, p. 042069, may 2022. [Online]. Available: https://dx.doi.org/10.1088/1742-6596/2265/4/042069

[12] F. Trevisi, C. E. D. Riboldi, and A. Croce, "Vortex model of the aerodynamic wake of airborne wind energy systems," *Wind Energy Science*, vol. 8, no. 6, pp. 999–1016, 2023.

[13] J. L. J. Pereira, G. A. Oliver, M. B. Francisco, S. S. Cunha, and G. F. Gomes, "A review of multi-objective optimization: Methods and algorithms in mechanical engineering problems," *Archives of Computational Methods in Engineering*, vol. 29, no. 4, pp. 2285–2308, 2022.

[14] R. Marler and J. Arora, "Survey of multi-objective optimization methods for engineering," *Structural and Multidisciplinary Optimization*, vol. 26, no. 6, pp. 369–395, 2004.

[15] P. K. Shukla and K. Deb, "On finding multiple pareto-optimal solutions using classical and evolutionary generating methods," *European Journal of Operational Research*, vol. 181, no. 3, pp. 1630–1652, 2007.

[16] N. Panagant, N. Pholdee, S. Bureerat, A. R. Yildiz, and S. Mirjalili, "A comparative study of recent multi-objective metaheuristics for solving constrained truss optimisation problems," *Archives of Computational Methods in Engineering*, vol. 28, no. 5, pp. 4031–4047, 2021.

[17] R. Kasimbeyli, Z. K. Ozturk, N. Kasimbeyli, G. D. Yalcin, and B. I. Erdem, "Comparison of some scalarization methods in multiobjective optimization: Comparison of scalarization methods," *Bulletin of the Malaysian Mathematical Sciences Society*, vol. 42, no. 5, pp. 1875–1905, 2019.

[18] I. Das and J. E. Dennis, "A closer look at drawbacks of minimizing weighted sums of objectives for pareto set generation in multicriteria optimization problems," *Structural optimization*, vol. 14, no. 1, pp. 63–69, 1997.

[19] A. Messac, A. Ismail-Yahaya, and C. Mattson, "The normalized normal constraint method for generating the pareto frontier," *Structural and Multidisciplinary Optimization*, vol. 25, no. 2, pp. 86–98, 2003.

[20] I. Das and J. E. Dennis, "Normal-boundary intersection: A new method for generating the pareto surface in nonlinear multicriteria optimization problems," *SIAM Journal on Optimization*, vol. 8, no. 3, pp. 631–657, 1998.

[21] A. Pascoletti and P. Serafini, "Scalarizing vector optimization problems," *Journal of Optimization Theory and Applications*, vol. 42, no. 4, pp. 499–524, 1984.